

## Discovery of a Single-Band Mott Insulator in a van der Waals Flat-Band Compound

Shunye Gao,<sup>1,2,3,||</sup> Shuai Zhang,<sup>1,2,||</sup> Cuixiang Wang,<sup>1,2,||</sup> Shaohua Yan,<sup>4,||</sup> Xin Han,<sup>1,2</sup> Xuecong Ji,<sup>1,2</sup> Wei Tao,<sup>1</sup> Jingtong Liu,<sup>1</sup> Tiantian Wang,<sup>1</sup> Shuaikang Yuan,<sup>1</sup> Gexing Qu,<sup>1,2</sup> Ziyang Chen,<sup>1,2</sup> Yongzhao Zhang,<sup>1,2</sup> Jierui Huang,<sup>1,2</sup> Mojun Pan,<sup>1,2</sup> Shiyu Peng,<sup>1,2</sup> Yong Hu,<sup>3</sup> Hang Li,<sup>3</sup> Yaobo Huang,<sup>5</sup> Hui Zhou,<sup>1,2</sup> Sheng Meng,<sup>1,2,6</sup> Liu Yang,<sup>7,8</sup> Zhiwei Wang,<sup>7,8,9</sup> Yugui Yao,<sup>7,8</sup> Zhiguo Chen,<sup>1,6</sup> Ming Shi,<sup>3,10</sup> Hong Ding,<sup>1,2,6</sup> Huaixin Yang,<sup>1,2,6</sup> Kun Jiang,<sup>1,2,6</sup> Yunliang Li,<sup>1,2,6</sup> Hechang Lei,<sup>4,\*</sup> Youguo Shi,<sup>1,2,6,†</sup> Hongming Weng,<sup>1,2,6,‡</sup> and Tian Qian<sup>1,6,§</sup>

<sup>1</sup>Beijing National Laboratory for Condensed Matter Physics and Institute of Physics, Chinese Academy of Sciences, Beijing 100190, China

<sup>2</sup>University of Chinese Academy of Sciences, Beijing 100049, China

<sup>3</sup>Photon Science Division, Paul Scherrer Institut, CH-5232 Villigen, Switzerland

<sup>4</sup>Department of Physics and Beijing Key Laboratory of Opto-electronic Functional Materials and Micro-nano Devices, Renmin University of China, Beijing 100872, China

<sup>5</sup>Shanghai Synchrotron Radiation Facility, Shanghai Advanced Research Institute, Chinese Academy of Sciences, Shanghai 201210, China

<sup>6</sup>Songshan Lake Materials Laboratory, Dongguan, Guangdong 523808, China

<sup>7</sup>Centre of Quantum Physics, Key Laboratory of Advanced Optoelectronic Quantum Architecture and Measurement, Ministry of Education, School of Physics, Beijing Institute of Technology, Beijing 100081, China

<sup>8</sup>Micronano Center, Beijing Key Lab of Nanophotonics and Ultrafine Optoelectronic Systems, Beijing Institute of Technology, Beijing 100081, China

<sup>9</sup>Material Science Center, Yangtze Delta Region Academy of Beijing Institute of Technology, Jiaxing 314011, China

<sup>10</sup>Center for Correlated Matter and Department of Physics, Zhejiang University, Hangzhou 310058, China



(Received 2 March 2023; revised 19 October 2023; accepted 31 October 2023; published 13 December 2023)

The Mott insulator provides an excellent foundation for exploring a wide range of strongly correlated physical phenomena, such as high-temperature superconductivity, quantum spin liquid, and colossal magnetoresistance. A Mott insulator with the simplest degree of freedom is an ideal and highly desirable system for studying the fundamental physics of Mottness. In this study, we have unambiguously identified such an anticipated Mott insulator in a van der Waals layered compound Nb<sub>3</sub>Cl<sub>8</sub>. In the high-temperature phase, where interlayer coupling is negligible, density functional theory calculations for the monolayer of Nb<sub>3</sub>Cl<sub>8</sub> suggest a half-filled flat band at the Fermi level, whereas angle-resolved photoemission spectroscopy experiments observe a large gap. This observation is perfectly reproduced by dynamical mean-field theory calculations considering strong electron correlations, indicating a correlation-driven Mott insulator state. Since this half-filled band derived from a single 2a<sub>1</sub> orbital is isolated from all other bands, the monolayer of Nb<sub>3</sub>Cl<sub>8</sub> is an ideal realization of the celebrated single-band Hubbard model. Upon decreasing the temperature, the bulk system undergoes a phase transition, where structural changes significantly enhance the interlayer coupling. This results in a bonding-antibonding splitting in the Hubbard bands, while the Mott gap remains dominant. Our discovery provides a simple and seminal model system for investigating Mott physics and other emerging correlated states.

DOI: 10.1103/PhysRevX.13.041049

Subject Areas: Condensed Matter Physics

\*Corresponding author: hlei@ruc.edu.cn

†Corresponding author: ygshi@iphy.ac.cn

‡Corresponding author: hmweng@iphy.ac.cn

§Corresponding author: tqian@iphy.ac.cn

||These authors contributed equally to this work.

Published by the American Physical Society under the terms of the Creative Commons Attribution 4.0 International license. Further distribution of this work must maintain attribution to the author(s) and the published article's title, journal citation, and DOI.

## I. INTRODUCTION

In solid-state physics, the classification of materials based on their transport properties is one of the oldest and least-understood problems. According to modern band theory, metals possess partially filled bands while insulators have all bands fully filled. However, this explanation is incomplete. The physics regarding partially filled bands faces significant challenges due to electron-electron correlations. One typical example is the formation of Mott

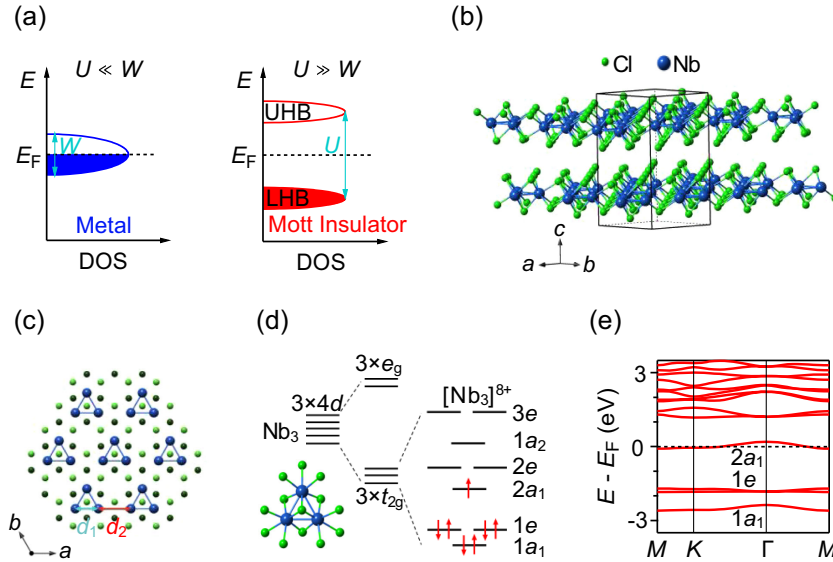


FIG. 1. Half-filled flat band in the monolayer of  $\alpha$ - $\text{Nb}_3\text{Cl}_8$ . (a) Schematic illustrations of a metal for  $U \ll W$  (left) and a Mott insulator for  $U \gg W$  (right). (b) Crystal structure of  $\alpha$ - $\text{Nb}_3\text{Cl}_8$ . (c) Top view of the monolayer of  $\text{Nb}_3\text{Cl}_8$  showing the  $\text{Nb}_3$  trimers. Blue lines indicate the Nb–Nb metal bonds within each  $\text{Nb}_3$  trimer. Dark- and light-green spheres represent the Cl atoms below and above the Nb layer, respectively. (d) Schematic illustration of the molecular orbitals in an isolated  $\text{Nb}_3\text{Cl}_{13}$  cluster, occupied by seven Nb 4d valence electrons for a  $[\text{Nb}_3]^{8+}$  trimer. Inset: top view of a  $\text{Nb}_3\text{Cl}_{13}$  cluster composed of three edge-sharing  $\text{NbCl}_6$  octahedra. (e) Calculated band structure of the monolayer of  $\text{Nb}_3\text{Cl}_8$  using the HSE06 functional.

insulators [1,2]. Mott physics is governed by two critical energy scales: the bandwidth ( $W$ ) and the correlation strength ( $U$ ). As illustrated in Fig. 1(a), for a half-filled system, if  $U \ll W$ , the system falls into the metallic band regime. Conversely, if  $U \gg W$ , the system transforms into a Mott insulator, where strong correlations split the metallic band into two: The lower band is filled while the upper one is empty. In Mott insulators, localized electrons are expected to carry local magnetic moments, often resulting in an antiferromagnetic ground state, as observed in the parent compounds of cuprate superconductors [3]. In addition, Mott insulators exhibit various magnetic ground states, such as spin singlet states [4,5], quantum spin liquid states [6], and valence bond states [7]. Numerous intriguing physical phenomena are triggered from Mott insulators, such as high-temperature superconductivity [3], colossal magnetoresistance [8,9], non-Fermi liquid [10], and so on. Many strongly correlated systems have been investigated within the framework of Mott physics, also known as Mottness, including the recently discovered insulator behavior and superconductivity in magic-angle twisted bilayer graphene [11,12].

The theoretical understanding for the Mott physics has been achieved using simplified models, in particular, the single-band Hubbard model, which considers electrons on one band in a single orbital [1]. However, low-energy excitations in real materials are usually complicated by various factors—such as multiple bands, orbital degeneracy, spin-orbit coupling, Peierls instability, and so on [13]—making experimental verification and theoretical analysis

challenging and controversial. Well-known examples are the parent compounds of cuprate superconductors, which feature a half-filled band at the Fermi level ( $E_F$ ), arising from a strong hybridization of the Cu  $3d_{x^2-y^2}$  orbital with the O  $2p_x$  and  $2p_y$  orbitals. Consequently, the low-energy excitations are described by the Zhang-Rice singlets emerging from the strong  $p$ - $d$  hybridization [14]. In the  $5d$  system  $\text{Sr}_2\text{IrO}_4$ , the partially filled wide  $t_{2g}$  states would lead to metallic behavior. Strong spin-orbit coupling is required to split the  $t_{2g}$  states, resulting in a separated half-filled band with a relatively narrow width [15]. The metal-insulator transition in  $\text{VO}_2$  is accompanied by a dimerization of the V atoms [4]. The origin of the insulating gap has been a subject of debate, whether it arises from bonding-antibonding splitting [16,17] or electron correlations [5,18–20]. In the charge-density-wave phase of  $1T$ - $\text{TaS}_2$ , band folding and hybridization result in a reconstructed flat band at  $E_F$  in the superlattice [21,22]. However, the interplay between interlayer coupling and electron correlations complicates the insulating behavior in  $1T$ - $\text{TaS}_2$  [23,24].

In this work, we have discovered a textbook example of the single-band Mott insulator in a van der Waals (vdW) compound  $\text{Nb}_3\text{Cl}_8$ . The electronic states in the high-temperature phase can be adequately described based on the monolayer of  $\text{Nb}_3\text{Cl}_8$ , as the interlayer coupling is negligible. Density functional theory (DFT) calculations show that the monolayer of  $\text{Nb}_3\text{Cl}_8$  features a single half-filled band derived from the  $2a_1$  orbital at  $E_F$ . This band exhibits a nearly flat dispersion with  $W \sim 0.3$  eV, which is significantly smaller than the typical  $U$  values on the order

of eV for Nb  $4d$  orbitals [25–28], indicating its strong correlation nature. Strong correlations drive the half-filled system to transform into a Mott insulator, resulting in a splitting of the half-filled band into lower and upper Hubbard bands (LHB and UHB). Since this half-filled  $2a_1$  band is well separated from other bands, the monolayer of  $\text{Nb}_3\text{Cl}_8$  can be ideally described by the single-band Hubbard model. Moreover, the Curie-Weiss paramagnetism observed in the high-temperature phase indicates the existence of spin-1/2 local moments, which is in excellent agreement with the prediction of the single-band Hubbard model.

As the temperature decreases, the bulk system undergoes a phase transition. In the low-temperature phase, the structural changes in the stacking sequence greatly enhance the interlayer coupling, leading to significant impacts on the correlated electronic states. A bonding-antibonding splitting occurs in the Hubbard bands, while the spins pair into interlayer spin singlets, resulting in nonmagnetic behavior. Despite these remarkable changes, the system remains in the Mott insulator regime in the low-temperature phase, as the insulating gap is still dominated by strong electron correlations.

## II. INSULATING STATE ON A HALF-FILLED BAND

In the high-temperature phase ( $\alpha$  phase) above  $T^* \sim 100$  K, each unit cell consists of two monolayers of  $\text{Nb}_3\text{Cl}_8$  stacked along the  $c$  axis via weak vdW forces [Fig. 1(b)] [29,30]. In each monolayer, the Nb ions form a breathing kagome lattice, where three Nb ions are in close proximity, constituting one  $\text{Nb}_3$  trimer [Fig. 1(c)] [29–31]. Each  $\text{Nb}_3$  trimer is surrounded by 13 Cl ions, forming a  $\text{Nb}_3\text{Cl}_{13}$  cluster composed of three edge-sharing  $\text{NbCl}_6$  octahedra [inset of Fig. 1(d)]. The intracluster Nb–Nb distance  $d_1 = 2.834$  Å is substantially shorter than the intercluster Nb–Nb distance  $d_2 = 3.998$  Å [32], indicating the formation of Nb–Nb metal bonds within each cluster. The octahedral crystal field splits the Nb  $4d$  orbitals into  $e_g$  and  $t_{2g}$  orbitals, which further divide into molecular orbitals due to the metal bonds, as illustrated in Fig. 1(d). The  $3p$  shell of the Cl ions is filled due to their strong electronegativity. Consequently, the  $\text{Nb}_3$  trimers in  $\text{Nb}_3\text{Cl}_8$  have a valence state of +8, with seven valence electrons occupying the molecular orbitals. Six valence electrons occupy the lowest three molecular orbitals, while the seventh electron resides in the  $2a_1$  orbital [29,30,33,34].

The occupied molecular orbitals correspond to four bands between  $-3$  and  $0.5$  eV in the DFT calculations shown in Fig. 1(e). Because of symmetry breaking and large lattice distortion in the breathing kagome lattice, the bands deviate significantly from the characteristic band structure of the conventional kagome lattice. The bandwidths are determined by the hybridization between

the Nb  $4d$  orbitals and the  $3p$  orbitals of the ligand Cl ions that bridge adjacent  $\text{Nb}_3$  trimers. The nearly flat band dispersions signify an extremely weak  $p$ - $d$  hybridization, in contrast to the strong  $p$ - $d$  hybridization in cuprates [14]. According to band theory, each filled band can accommodate two electrons. As a result, the half-filled  $2a_1$  band, which is occupied by one electron, is pinned at  $E_F$  in the DFT calculations.

The band structure obtained within the single-particle approximation suggests that  $\alpha$ - $\text{Nb}_3\text{Cl}_8$  exhibits a metallic state with a half-filled band at  $E_F$  [Fig. 2(a)]. In contrast, the angle-resolved photoemission spectroscopy (ARPES) results reveal a clear gap, as shown in Fig. 2(b). Despite performing the ARPES experiments at room temperature, the spectra are affected by charging effects. Specifically, the kinetic energy of photoelectrons decreases with increasing photon flux. The charging effects suggest that the samples exhibit highly insulating behavior, which is consistent with previous transport measurements [35]. By measuring the kinetic energy with different beamline slit sizes, which are proportional to photon flux, we determine that the valence band top at the  $\Gamma$  point is located  $0.7$  eV below  $E_F$  (see Fig. S1 in Supplemental Material [36]).

Except the half-filled band, the bands resolved by ARPES measurements show excellent consistency with the DFT calculations over a wide energy range. The calculations in Fig. 2(a) reveal that the valence band structure consists of two well-separated sets of bands. One set originates from the Cl  $3p$  orbitals and lies well below  $E_F$  due to the strong electronegativity, while the other set, with lower binding energies, originates from the Nb  $4d$  orbitals. The photon energy ( $h\nu$ )-dependent data in Fig. 2(c) show significant suppression of the spectral intensities of the bands within  $3$  eV below  $E_F$  around  $h\nu = 32$  eV, which corresponds to the binding energy of the Nb  $4p$  orbitals [see Fig. S5(d) in Supplemental Material [36]]. This behavior is attributed to the Nb  $4p$ - $4d$  antiresonance, similar to the Fe  $3p$ - $3d$  antiresonance observed in iron-based superconductors [37,38], confirming that these bands originate from the Nb  $4d$  orbitals.

Although the ARPES results reveal a clear gap at  $E_F$ , they do not provide information on the gap size because the bands above  $E_F$  cannot be detected in the ARPES experiments. To determine the gap size at  $E_F$ , we performed photoluminescence (PL) experiments. We note that PL spectra may also exhibit signals related to excitonic or impurity states. The PL spectrum excited by  $1.1$ -eV photons exhibits two peaks at  $0.7$  and  $1.0$  eV, respectively [Fig. 2(d)]. However, the  $0.7$ -eV peak vanishes when directly excited by  $0.75$ -eV photons, as shown in Fig. 2(e). The results suggest that the  $0.7$ -eV peak does not originate from intrinsic bands or impurity states. Instead, it is likely associated with an excitonic state formed by the Coulomb interactions between photo-excited electrons and holes during the optical excitation

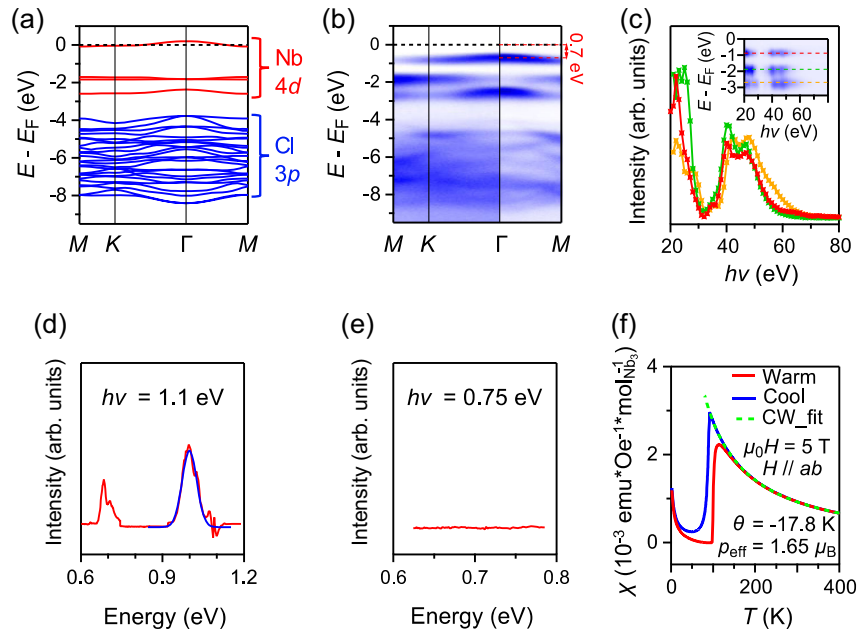


FIG. 2. Band gap at  $E_F$  revealed by ARPES and PL spectra. (a) Calculated valence band structure of the monolayer of  $\text{Nb}_3\text{Cl}_8$  using the HSE06 functional. Red and blue curves represent the bands originating from the Nb  $4d$  and Cl  $3p$  orbitals, respectively. (b) Intensity plot of the ARPES data along  $M-K-\Gamma-M$ . (c)  $h\nu$  dependence of the spectral intensities at three constant energies indicated by the dashed lines in the inset. Inset: intensity plot of the ARPES data at the  $M$  point with varying  $h\nu$ . The spectral intensities are normalized by photon flux. (d) PL spectrum excited by 1.1-eV photons (red curve). Stray signals caused by the incident light have been subtracted (see Fig. S3 in Supplemental Material [36]). The peak at 1.0 eV is fitted to a Gaussian function (blue curve). (e) Same as in (d) but excited by 0.75-eV photons. (f) Temperature-dependent magnetic susceptibility measured upon cooling (blue) and warming (red). The green dashed curve represents a fitting of the cooling data from 100 to 400 K to the Curie-Weiss function.

process. The 1.0-eV peak is attributed to the recombination of photoexcited electrons at the conduction band bottom and holes at the valence band top, indicating a gap size of 1.0 eV in  $\alpha\text{-Nb}_3\text{Cl}_8$  [see Fig. S2(b) in Supplemental Material [36]].

### III. MOTT INSULATOR DESCRIBED BY SINGLE-BAND HUBBARD MODEL

The observed insulating state with a large gap at  $E_F$  in  $\alpha\text{-Nb}_3\text{Cl}_8$  contradicts the metallic state predicted by the DFT calculations within the single-particle approximation. In a previous report, the ARPES results also showed an insulating state, which was interpreted as a band insulator by assuming that  $E_F$  lies within the band gap above the calculated half-filled band [39]. Under this assumption, this band should be fully occupied by two electrons, resulting in a total of eight valence electrons filling four Nb  $4d$  bands. However, this interpretation contradicts the fact that each  $[\text{Nb}_3]^{8+}$  trimer possesses seven valence electrons.

To elucidate the origin of the insulating state, we extract the experimental band dispersions and compare them with the band structure calculated using the Heyd-Scuseria-Ernzerhof (HSE06) hybrid functional in Fig. 3(a). Four bands are identified within 3 eV below  $E_F$  in the ARPES data [see Figs. S5(a) and S5(b) in Supplemental

Material [36]]. The lower three bands exhibit excellent consistency with the DFT calculations, signifying an accurate description within the single-particle approximation. However, a notable discrepancy arises in the topmost band between experiment and calculation. The calculations suggest a half-filled  $2a_1$  band at  $E_F$ , whereas the ARPES data show it well below  $E_F$ . In addition, the calculated  $2a_1$  band needs to be renormalized by a factor of 1.6 to match the experimental data [see Fig. S5(c) in Supplemental Material [36]], highlighting the importance of strong correlation effects on this band beyond the single-particle approximation. The half-filled band has a nearly flat dispersion with  $W \sim 0.3$  eV, while typical  $U$  values on Nb  $4d$  orbitals are on the order of eV [25–28]. Given that  $U$  is much larger than  $W$  on this half-filled band, it is thus reasonable to expect a correlation-driven Mott transition to occur, resulting in the observed insulating state. In the Mott insulator scenario, the localized electron in the  $2a_1$  orbital carries an unpaired spin, resulting in a local magnetic moment of  $S = 1/2$ . This expectation is supported by the magnetic susceptibility data, showing paramagnetic behavior in the  $\alpha$  phase [Fig. 2(f)]. The paramagnetic susceptibility is well fitted to the Curie-Weiss function, yielding an effective paramagnetic Bohr magneton of  $p_{\text{eff}} = 1.65 \mu_B$ , which is consistent with the theoretical value of  $1.73 \mu_B$  for  $S = 1/2$ .

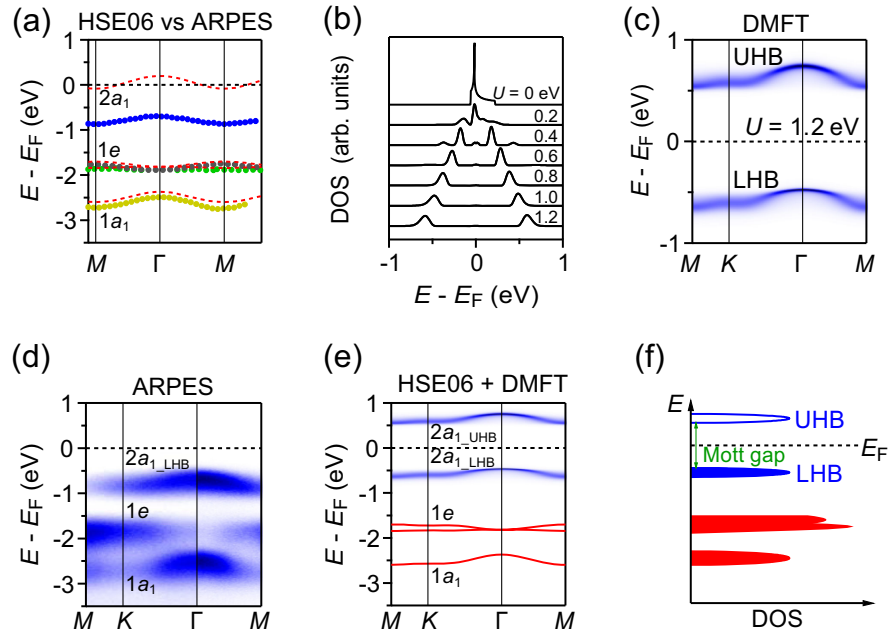


FIG. 3. Single-band Mott insulator state in  $\alpha\text{-Nb}_3\text{Cl}_8$ . (a) Comparison between the calculated and experimental bands. Red dashed curves represent the calculated bands based on the HSE06 functional. The experimental bands are extracted by tracking the peak positions of energy distribution curves in the ARPES data. Raw ARPES data are shown in Figs. S5(a) and S5(b) in the Supplemental Material [36]. (b) Density of states (DOS) of the single-band Hubbard model with increasing  $U$  from 0 to 1.2 eV. (c) Spectral function of the LHB and UHB along the high-symmetry path with  $U = 1.2$  eV. (d) Intensity plot of the ARPES data along  $M-K-\Gamma-M$ . (e) Combined band structure from the HSE06 (red) and DMFT (blue) calculations, which nearly perfectly reproduces the ARPES data in (d). (f) Schematic illustration of the electronic structure of  $\alpha\text{-Nb}_3\text{Cl}_8$ , showing a single-band Mott insulator state.

To account for the insulating state in  $\alpha\text{-Nb}_3\text{Cl}_8$ , electron correlation effects have been considered in previous spin-polarized DFT calculations, where long-range ferromagnetic or antiferromagnetic order was assumed [29,40,41]. However, the resulting magnetically ordered insulating states are inconsistent with the observed paramagnetic behavior in  $\alpha\text{-Nb}_3\text{Cl}_8$ . The static mean-field approximation in DFT +  $U$  calculations is inadequate to describe the Mott physics in this material. Therefore, we employed dynamical mean-field theory (DMFT) calculations for this half-filled band within the Hubbard model. This low-energy physical model is justified because the half-filled  $2a_1$  band is isolated from other bands, which have been well described within the single-particle approximation.

In the single-band Hubbard model, the electronic states undergo significant changes with increasing  $U$  [Fig. 3(b)]. When  $U$  exceeds 0.6 eV, the coherent part at  $E_F$  diminishes to negligible levels, while the incoherent part becomes well separated from  $E_F$ . This indicates that strong correlations drive a Mott transition, splitting the half-filled metallic band into LHB and UHB, with  $E_F$  located within the Mott gap between them. In Mott insulators,  $U$  determines the magnitude of the splitting between the LHB and UHB, which corresponds to the energy difference between the centers of the two bands [see Fig. S2(c) in Supplemental Material [36]]. The value of  $U$  can be estimated using the simple formula  $U = \Delta + (W_1 + W_2)/2$ , where  $\Delta$  is the

gap size between the top of the LHB and the bottom of the UHB, and  $W_1$  and  $W_2$  are the widths of the LHB and UHB, respectively. The PL spectrum in Fig. 2(d) has identified  $\Delta$  as 1.0 eV. The LHB and UHB should have similar widths since both of them arise from the splitting of the half-filled band [13]. The ARPES data show that  $W_1$  is about 0.2 eV, and therefore we assume that  $W_2$  is also about 0.2 eV. The estimated value of  $U \sim 1.2$  eV based on our experimental results agrees well with the calculated value of  $U \sim 1.15$  eV, which takes the nonlocal Coulomb interactions into account [42].

Figure 3(c) presents the spectral function of the single-band Hubbard model at  $U = 1.2$  eV, showing a splitting of the half-filled band into LHB and UHB, with the magnitude of the splitting determined by  $U$ . The noninteracting half-filled band needs to be renormalized by a factor of 1.7 when compared with the LHB and UHB, which is consistent with the experimental observation. The PL spectrum indicates a Mott gap size of 1.0 eV, while the ARPES data show that the top of the LHB lies 0.7 eV below  $E_F$ , suggesting that  $E_F$  does not coincide with the middle of the Mott gap in actual samples. Similar behavior has been observed in the parent compounds of cuprate superconductors [43–45]. The ARPES results in Fig. 3(d) are nearly perfectly reproduced by the combined band structure from the HSE06 and DMFT calculations in Fig. 3(e). The half-filled single band splits into LHB and UHB due to strong correlations, while

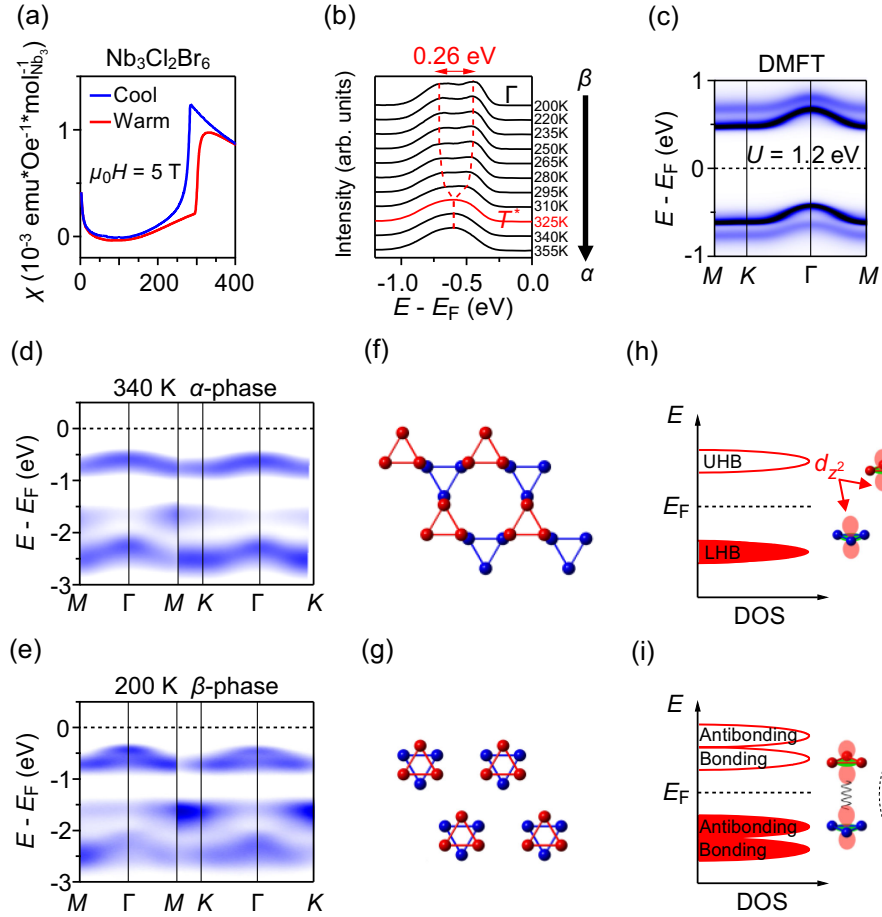


FIG. 4. Electronic structure changes between the  $\alpha$  and  $\beta$  phases in  $\text{Nb}_3\text{Cl}_2\text{Br}_6$ . (a) Temperature-dependent magnetic susceptibility measured upon cooling (blue) and warming (red). (b) Energy distribution curves at the  $\Gamma$  point measured at different temperatures upon warming. Red dashed curves are guides to the eye for the peak positions, showing a splitting of the LHB below  $T^*$ . (c) Spectral function of the bilayer of  $\beta\text{-Nb}_3\text{Cl}_8$  calculated by DMFT with  $U = 1.2$  eV and  $t_{\perp} = 0.1$  eV, showing the splitting of both LHB and UHB. (d,e) Intensity plots of the ARPES data along  $\Gamma - M - K - \Gamma$  collected at 340 and 200 K, respectively. (f,g) Top view of the  $\text{Nb}_3$  trimers of one bilayer in the  $\alpha$  and  $\beta$  phases, respectively. Red and blue circles indicate the Nb ions in the top and bottom monolayers, respectively. (h,i) Schematic illustrations of the electronic structures in the  $\alpha$  and  $\beta$  phases, respectively. The insets show the  $d_{z^2}$  orbitals of the  $\text{Nb}_3$  trimers in the bilayer, which are staggered in the  $\alpha$  phase (h), but directly on top in the  $\beta$  phase to form an interlayer spin singlet (i).

other bands are well described within the single-particle approximation, as illustrated in Fig. 3(f). The excellent agreement demonstrates that  $\alpha\text{-Nb}_3\text{Cl}_8$  is an ideal Mott insulator described by the single-band Hubbard model. In addition, in the Hubbard model, the exchange coupling  $J = -4t^2/U$  is estimated to be  $-2.4$  meV, with the nearest-neighbor hopping parameter  $t$  estimated to be  $0.027$  eV within the tight-binding approximation. The  $J$  value is comparable to the  $k_B\theta$  value of  $-1.5$  meV determined from the magnetic susceptibility data in Fig. 2(f), with  $\theta = -17.8$  K representing the Curie-Weiss temperature.

#### IV. MOTT INSULATOR STATE IN $\beta$ PHASE

As the temperature decreases,  $\text{Nb}_3\text{Cl}_8$  undergoes a transition from the paramagnetic  $\alpha$  phase to the nonmagnetic  $\beta$  phase at  $T^* \sim 100$  K, accompanied by

significant structural changes [29,30]. The existence of a nonmagnetic ground state is unusual, as Mott insulators usually exhibit magnetically ordered states at low temperatures. The nonmagnetic state has been proposed to arise from either spin singlet [29] or  $[\text{Nb}_3]^{7+} - [\text{Nb}_3]^{9+}$  charge disproportionation [30]. An essential question is whether the Mott physics remains significant in the nonmagnetic state. To address this, it is necessary to investigate the electronic structure of the  $\beta$  phase. However, because of the highly insulating nature at low temperatures, it is not possible to obtain the electronic structure of  $\beta\text{-Nb}_3\text{Cl}_8$  with ARPES. Fortunately, the  $\alpha$  to  $\beta$  phase transition temperature  $T^*$  can be tuned from about 100 K to 400 K in the  $\text{Nb}_3\text{Cl}_{8-x}\text{Br}_x$  series with increasing  $x$  [46]. Therefore, we synthesize  $\text{Nb}_3\text{Cl}_2\text{Br}_6$  samples, where  $T^*$  is near room temperature [Fig. 4(a)]. This method allows us to investigate the changes in the electronic

structure across  $T^*$  through temperature-dependent ARPES measurements.

The ARPES data in Fig. 4(d) reveal that the band structure of  $\alpha$ - $\text{Nb}_3\text{Cl}_2\text{Br}_6$  closely resembles that of  $\alpha$ - $\text{Nb}_3\text{Cl}_8$  (see Fig. S7 in Supplemental Material for more details [36]), confirming  $\alpha$ - $\text{Nb}_3\text{Cl}_2\text{Br}_6$  as a single-band Mott insulator. The most notable change in the band structure is the splitting of the LHB in the  $\beta$  phase, as shown in Fig. 4(e). The temperature-dependent data in Fig. 4(b) show that the splitting occurs at  $T^*$ , confirming that it arises from the phase transition. However, no discernible changes are observed in the core level peak of the Nb 4s orbital across  $T^*$  (see Fig. S8 in Supplemental Material [36]), indicating a lack of variation in the valence state of the Nb ions. This observation contradicts the suggested  $[\text{Nb}_3]^{7+} - [\text{Nb}_3]^{9+}$  charge disproportionation [30].

Previous studies have reported significant changes in the stacking sequence of  $\text{Nb}_3\text{Cl}_8$  layers between  $\alpha$  and  $\beta$  phases [29,30,46]. In the  $\alpha$  phase, the  $\text{Nb}_3$  trimers are staggered between adjacent monolayers [Fig. 4(f)], while in the  $\beta$  phase, they stack directly on top of each other within each bilayer [Fig. 4(g)]. Previous DFT calculations have suggested that the structural changes effectively enhance the interlayer coupling of the  $\text{Nb}_3$  trimers [29,47]. To investigate the effects on the Mott insulator state, we perform DMFT calculations for the bilayer of  $\beta$ - $\text{Nb}_3\text{Cl}_8$ , considering the interlayer coupling  $t_\perp$ , while assuming that  $U$  remains constant across the phase transition. The value of  $t_\perp$  is estimated to be 0.1 eV, which is half of the splitting at the  $\Gamma$  point calculated by DFT [see Fig. S10(b) in Supplemental Material [36]]. We note that substituting Cl with Br does not significantly affect the interlayer coupling strength [47]. As shown in Fig. 4(c), the DMFT calculations reveal an energy splitting of both LHB and UHB in the bilayer of  $\beta$ - $\text{Nb}_3\text{Cl}_8$ , in good agreement with the ARPES data in Fig. 4(e). Therefore, the splitting arises from the enhanced interlayer hybridization, leading to the formation of bonding-antibonding states in the  $\beta$  phase.

The strong interlayer hybridization within the bilayer in the nonmagnetic  $\beta$  phase is reminiscent of the observation in  $\text{VO}_2$ , where a nonmagnetic insulating phase emerges when the V atoms dimerize [4,5,48]. However, it remains unclear whether the insulating gap in  $\text{VO}_2$  arises from bonding-antibonding splitting [16,17] or electron correlations [5,18–20], i.e., a Peierls-type band insulator or a Mott insulator. Our ARPES data reveal in  $\beta$ - $\text{Nb}_3\text{Cl}_2\text{Br}_6$  that the splitting magnitude of 0.26 eV in the LHB is much smaller than the Mott gap size of 1.0 eV. It is evident that the bonding-antibonding splitting has minor effects on the Mott gap, and consequently, the insulating gap is dominantly determined by  $U$ , as illustrated in Fig. 4(i). Therefore, the  $\beta$  phase still falls within the Mott insulator regime.

The nonmagnetic behavior suggests that the spin-1/2 magnetic moments are quenched in the  $\beta$  phase. In the

on-top stacked  $\text{Nb}_3$  trimers, a pair of spins is likely to couple antiferromagnetically, forming an interlayer spin singlet in the bonding-antibonding states, as illustrated in Fig. 4(i). This results in a spin-singlet Mott insulator state that exhibits nonmagnetic behavior. Therefore, despite the drastic changes in the magnetic properties, the Mott physics plays a dominant role in both the  $\alpha$  and  $\beta$  phases.

## V. SUMMARY AND OUTLOOK

Our results firmly establish  $\alpha$ - $\text{Nb}_3\text{Cl}_8$  as a canonical spin-1/2 Mott insulator arising from a half-filled flat band with  $U \gg W$ . Since this band, derived from a single  $2a_1$  orbital, is isolated from the high-energy bands, the Mott insulator state can be ideally described by the single-band Hubbard model. The localization of electrons in the  $\text{Nb}_3$  trimers, due to the long distance between them, suppresses the electronic kinetic energy, leading to a Mott transition. This transition straightforwardly manifests the Mott physics envisioned in Mott's thought experiment [2].

Given the numerous intriguing physical phenomena that have emerged from Mott insulators, there is a strong motivation to manipulate the Mott insulator state in  $\text{Nb}_3\text{Cl}_8$ , as well as in related systems like  $\text{Nb}_3\text{Br}_8$  and  $\text{Nb}_3\text{I}_8$ , through various methods such as doping, pressure, magnetic fields, and optical pulses. Because of the weak vdW coupling,  $\text{Nb}_3\text{Cl}_8$  crystals can be easily exfoliated into few-layer or even monolayer flakes [35,39], making it convenient to study and utilize the Mott insulator state [49,50]. For instance, a magnetic-field-free Josephson diode has been recently achieved in a vdW heterostructure based on its sister material  $\text{Nb}_3\text{Br}_8$  [51,52]. It is feasible and desirable to fabricate Mott insulator-based devices with this family of materials to produce more exotic quantum phenomena. A previous study has revealed that the transition from the  $\alpha$  to  $\beta$  phase is entirely suppressed in thin flakes, resulting in the paramagnetic state persisting down to 2 K [30]. While the calculations suggest a  $120^\circ$  antiferromagnetic ground state in the monolayer [42], geometric frustration in the triangular lattices formed by the spin-1/2  $\text{Nb}_3$  trimers may lead to more exotic ground states, such as a quantum spin liquid or resonating valence bond state. Lastly, flat-band systems, characterized by a high density of states at  $E_F$  and quenched electronic kinetic energy, are considered a fertile ground for strongly correlated phases of matter [41,53–55]. The Mott insulator state derived from a single flat band makes  $\text{Nb}_3\text{Cl}_8$  a paradigmatic system that exemplifies strongly correlated physical phenomena resulting from flat-band effects. Our discovery will stimulate intensive exploration of the flat-band effects in the materials database.

## ACKNOWLEDGMENTS

We thank X.-Z. Chen, B. Jiang, M.-Z. Hu, F.-M. Chen, J.-D. Liu, I. Vobornik, J. Fujii, N. C. Plumb, A. Pfister,

H.-E. Zhu, C. Polley, and N. Olszowska for technical assistance. This work was supported by the Ministry of Science and Technology of China (Grants No. 2022YFA1403800, No. 2018YFA0305700, No. 2018YFE0202600, No. 2020YFA0308800, and No. 2022YFA1403401), the National Natural Science Foundation of China (Grants No. U22A6005, No. U1832202, No. 11925408, No. 11921004, No. 12188101, No. U2032204, No. 12274459, No. 22073111, No. 92250307, No. 12174428, No. 12061131002, No. 11888101, No. U21A20432, No. 12321004, No. 12025407, and No. 92065109), the Chinese Academy of Sciences (Grants No. QYZDB-SSW-SLH043, No. XDB33000000, and No. XDB28000000), the Informatization Plan of Chinese Academy of Sciences (Grant No. CAS-WX2021SF-0102), the Beijing Natural Science Foundation (Grants No. Z210006 and No. Z200005), the China Scholarship Council (Grant No. 202104910090), the Sino-Swiss Science and Technology Cooperation (Grant No. CN-EG-03-012021), the Swiss National Science Foundation (Grant No. 200021-188413), the Fundamental Research Funds for the Central Universities and Research Funds of Renmin University of China (RUC) (Grants No. 18XNLG14, No. 19XNLG13, and No. 19XNLG17), the Outstanding Innovative Talents Cultivation Funded Programs 2022 of Renmin University of China, and the Beijing National Laboratory for Condensed Matter Physics. We acknowledge the Synergetic Extreme Condition User Facility (SECUF), the “Dreamline” beamline of Shanghai Synchrotron Radiation Facility (SSRF), the Steady High Magnetic Field Facility (SHMFF), the SIS-ULTRA beamline of the Swiss Light Source, the APE-LE beamline of the Elettra Light Source (Proposal No. 20215821), the 13U ARPES beamline of the National Synchrotron Radiation Laboratory in Hefei (Proposal No. 2021-HLS-PT-004344), the “Bloch” beamline of MAXIV in Sweden (Proposal No. 20200353), and the “UARPE” beamline of SOLARIS in Poland (Proposal No. 211070).

---

[1] J. Hubbard, *Electron correlations in narrow energy bands*, *Proc. R. Soc. A* **276**, 238 (1963).  
 [2] N. F. Mott, *Metal-insulator transitions*, *Rev. Mod. Phys.* **40**, 677 (1968).  
 [3] P. A. Lee, N. Nagaosa, and X.-G. Wen, *Doping a Mott insulator: Physics of high-temperature superconductivity*, *Rev. Mod. Phys.* **78**, 17 (2006).  
 [4] J. P. Pouget, H. Launois, T. M. Rice, P. Dernier, A. Gossard, G. Villeneuve, and P. Hagenmuller, *Dimerization of a linear Heisenberg chain in the insulating phases of  $V_{1-x}Cr_xO_2$* , *Phys. Rev. B* **10**, 1801 (1974).  
 [5] T. J. Huffman, C. Hendriks, E. J. Walter, J. Yoon, H. Ju, R. Smith, G. L. Carr, H. Krakauer, and M. M. Qazilbash, *Insulating phases of vanadium dioxide are Mott-Hubbard insulators*, *Phys. Rev. B* **95**, 075125 (2017).

[6] A. Pustogow *et al.*, *Quantum spin liquids unveil the genuine Mott state*, *Nat. Mater.* **17**, 773 (2018).  
 [7] M. Tamura, A. Nakao, and R. Kato, *Frustration-induced valence-bond ordering in a new quantum triangular antiferromagnet based on  $[Pd(dmit)_2]$* , *J. Phys. Soc. Jpn.* **75**, 093701 (2006).  
 [8] S. Jin, T. H. Tiefel, M. McCormack, R. A. Fastnacht, R. Ramesh, and L. H. Chen, *Thousandfold change in resistivity in magnetoresistive La – Ca – Mn – O films*, *Science* **264**, 413 (1994).  
 [9] M. B. Salamon and M. Jaime, *The physics of manganites: Structure and transport*, *Rev. Mod. Phys.* **73**, 583 (2001).  
 [10] G. R. Stewart, *Non-Fermi-liquid behavior in  $d$ - and  $f$ -electron metals*, *Rev. Mod. Phys.* **73**, 797 (2001).  
 [11] Y. Cao *et al.*, *Correlated insulator behaviour at half-filling in magic-angle graphene superlattices*, *Nature (London)* **556**, 80 (2018).  
 [12] Y. Cao, V. Fatemi, S. Fang, K. Watanabe, T. Taniguchi, E. Kaxiras, and P. Jarillo-Herrero, *Unconventional superconductivity in magic-angle graphene superlattices*, *Nature (London)* **556**, 43 (2018).  
 [13] M. Imada, A. Fujimori, and Y. Tokura, *Metal-insulator transitions*, *Rev. Mod. Phys.* **70**, 1039 (1998).  
 [14] F. C. Zhang and T. M. Rice, *Effective Hamiltonian for the superconducting Cu oxides*, *Phys. Rev. B* **37**, 3759(R) (1988).  
 [15] B. J. Kim *et al.*, *Novel  $J_{\text{eff}} = 1/2$  Mott state induced by relativistic spin-orbit coupling in  $Sr_2IrO_4$* , *Phys. Rev. Lett.* **101**, 076402 (2008).  
 [16] R. M. Wentzcovitch, W. W. Schulz, and P. B. Allen,  *$VO_2$ : Peierls or Mott-Hubbard? A view from band theory*, *Phys. Rev. Lett.* **72**, 3389 (1994).  
 [17] V. Eyert,  *$VO_2$ : A novel view from band theory*, *Phys. Rev. Lett.* **107**, 016401 (2011).  
 [18] T. M. Rice, H. Launois, and J. P. Pouget, *Comment on “ $VO_2$ : Peierls or Mott-Hubbard? A view from band theory”*, *Phys. Rev. Lett.* **73**, 3042 (1994).  
 [19] A. X. Gray *et al.*, *Correlation-driven insulator-metal transition in near-ideal vanadium dioxide films*, *Phys. Rev. Lett.* **116**, 116403 (2016).  
 [20] O. Nájera, M. Civelli, V. Dobrosavljević, and M. J. Rozenberg, *Resolving the  $VO_2$  controversy: Mott mechanism dominates the insulator-to-metal transition*, *Phys. Rev. B* **95**, 035113 (2017).  
 [21] P. Fazekas and E. Tosatti, *Electrical, structural and magnetic properties of pure and doped 1T-TaS<sub>2</sub>*, *Philos. Mag. B* **39**, 229 (1979).  
 [22] K. Rossnagel and N. V. Smith, *Spin-orbit coupling in the band structure of reconstructed 1T-TaS<sub>2</sub>*, *Phys. Rev. B* **73**, 073106 (2006).  
 [23] Y. D. Wang, W. L. Yao, Z. M. Xin, T. T. Han, Z. G. Wang, L. Chen, C. Cai, Y. Li, and Y. Zhang, *Band insulator to Mott insulator transition in 1T-TaS<sub>2</sub>*, *Nat. Commun.* **11**, 4215 (2020).  
 [24] C. Wen *et al.*, *Roles of the narrow electronic band near the Fermi level in 1T-TaS<sub>2</sub>-related layered materials*, *Phys. Rev. Lett.* **126**, 256402 (2021).  
 [25] E. Sasioglu, C. Friedrich, and S. Blugel, *Effective Coulomb interaction in transition metals from constrained random-phase approximation*, *Phys. Rev. B* **83**, 121101(R) (2011).

- [26] E. G. C. P. van Loon, M. Rösner, G. Schönhoff, M. I. Katsnelson, and T. O. Wehling, *Competing Coulomb and electron-photon interactions in NbS<sub>2</sub>*, *npj Quantum Mater.* **3**, 32 (2018).
- [27] W. Wang, B. Wang, Z. Gao, G. Tang, W. Lei, X. Zheng, H. Li, X. Ming, and C. Autieri, *Charge density wave instability and pressure-induced superconductivity in bulk 1T-NbS<sub>2</sub>*, *Phys. Rev. B* **102**, 155115 (2020).
- [28] L. Craco and D. Leoni, *Mott and pseudogap localization in pressurized NbO<sub>2</sub>*, *Phys. Rev. B* **102**, 045142 (2020).
- [29] J. P. Sheckelton, K. W. Plumb, B. A. Trump, C. L. Broholm, and T. M. McQueen, *Rearrangement of van der Waals stacking and formation of a singlet state at T = 90K in a cluster magnet*, *Inorg. Chem. Front.* **4**, 481 (2017).
- [30] Y. Haraguchi, C. Michioka, M. Ishikawa, Y. Nakano, H. Yamochi, H. Ueda, and K. Yoshimura, *Magnetic-nonmagnetic phase transition with interlayer charge disproportionation of Nb<sub>3</sub> trimers in the cluster compound Nb<sub>3</sub>Cl<sub>8</sub>*, *Inorg. Chem.* **56**, 3483 (2017).
- [31] S. N. Magonov, P. Zoennchen, H. Rotter, H. J. Cantow, G. Thiele, J. Ren, and M. H. Whangbo, *Scanning tunneling and atomic force microscopy study of layered transition metal halides Nb<sub>3</sub>X<sub>8</sub> (X = Cl, Br, I)*, *J. Am. Chem. Soc.* **115**, 2495 (1993).
- [32] M. Ströbele, J. Glaser, A. Lachgar, and H.-J. Meyer, *Structure and electrochemical study of Nb<sub>3</sub>Cl<sub>8</sub>*, *Z. Anorg. Allg. Chem.* **627**, 2002 (2001).
- [33] J. R. Kennedy, P. Adler, R. Dronskowski, and A. Simon, *Experimental and theoretical electronic structure investigations on  $\alpha$ -Nb<sub>3</sub>Cl<sub>8</sub> and the intercalated phase  $\beta'$ -NaNb<sub>3</sub>Cl<sub>8</sub>*, *Inorg. Chem.* **35**, 2276 (1996).
- [34] G. Chen, H. Kee, and Y. B. Kim, *Cluster Mott insulators and two Curie-Weiss regimes on an anisotropic kagome lattice*, *Phys. Rev. B* **93**, 245134 (2016).
- [35] J. Yoon, E. Lesne, K. Sklarek, J. Sheckelton, C. Pasco, S. S. P. Parkin, T. M. McQueen, and M. N. Ali, *Anomalous thickness-dependent electrical conductivity in van der Waals layered transition metal halide, Nb<sub>3</sub>Cl<sub>8</sub>*, *J. Phys. Condens. Matter* **32**, 304004 (2020).
- [36] See Supplemental Material at <http://link.aps.org/supplemental/10.1103/PhysRevX.13.041049> for “Discovery of a single-band Mott insulator in a van der Waals flat-band compound.”
- [37] T. Qian *et al.*, *Quasinested Fe orbitals versus Mott-insulating V orbitals in superconducting Sr<sub>2</sub>VFeAsO<sub>3</sub> as seen from angle-resolved photoemission*, *Phys. Rev. B* **83**, 140513(R) (2011).
- [38] H. Ding *et al.*, *Electronic structure of optimally doped pnictide Ba<sub>0.6</sub>K<sub>0.4</sub>Fe<sub>2</sub>As<sub>2</sub>: A comprehensive angle-resolved photoemission spectroscopy investigation*, *J. Phys. Condens. Matter* **23**, 135701 (2011).
- [39] Z. Sun *et al.*, *Observation of topological flat bands in the kagome semiconductor Nb<sub>3</sub>Cl<sub>8</sub>*, *Nano Lett.* **22**, 4596 (2022).
- [40] J. Jiang, Q. Liang, R. Meng, Q. Yang, C. Tan, X. Sun, and X. Chen, *Exploration of new ferromagnetic, semiconductor and biocompatible Nb<sub>3</sub>X<sub>8</sub> (X = Cl, Br or I) monolayers with considerable visible and infrared light absorption*, *Nanoscale* **9**, 2992 (2017).
- [41] H. Liu, S. Meng, and F. Liu, *Screening two-dimensional materials with topological flat bands*, *Phys. Rev. Mater.* **5**, 084203 (2021).
- [42] S. Crytsiuk, M. I. Katsnelson, E. G. C. P. van Loon, and M. Rösner, *Nb<sub>3</sub>Cl<sub>8</sub>: A prototypical layered Mott-Hubbard insulator*, *arXiv:2305.04854*.
- [43] C. Ye, P. Cai, R. Yu, X. Zhou, W. Ruan, Q. Liu, C. Jin, and Y. Wang, *Visualizing the atomic-scale electronic structure of the Ca<sub>2</sub>CuO<sub>2</sub>Cl<sub>2</sub> Mott insulator*, *Nat. Commun.* **4**, 1365 (2013).
- [44] W. Ruan *et al.*, *Relationship between the parent charge transfer gap and maximum transition temperature in cuprates*, *Sci. Bull.* **61**, 1826 (2016).
- [45] C. Hu *et al.*, *Momentum-resolved visualization of electronic evolution in doping a Mott insulator*, *Nat. Commun.* **12**, 1356 (2021).
- [46] C. M. Pasco, I. E. Baggari, E. Bianco, L. F. Kourkoutis, and T. M. McQueen, *Tunable magnetic transition to a singlet ground state in a 2D van der Waals layered trimerized kagome magnet*, *ACS Nano* **13**, 9457 (2019).
- [47] Y. Zhang, Y. Gu, H. Weng, K. Jiang, and J. Hu, *Mottness in two-dimensional van der Waals Nb<sub>3</sub>X<sub>8</sub> monolayers (X = Cl, Br, and I)*, *Phys. Rev. B* **107**, 035126 (2023).
- [48] F. J. Morin, *Oxides which show a metal-to-insulator transition at the Neel temperature*, *Phys. Rev. Lett.* **3**, 34 (1959).
- [49] G. Cantele, F. Conte, L. Zullo, and D. Ninno, *Tunable electronic and magnetic properties of thin Nb<sub>3</sub>I<sub>8</sub> nanofilms: Interplay between strain and thickness*, *Phys. Rev. B* **106**, 085418 (2022).
- [50] Z. Jiang *et al.*, *Pressure-driven symmetry breaking and electron disproportionation of the trigonal Nb<sub>3</sub> cluster in Nb<sub>3</sub>Cl<sub>8</sub>*, *Sci. China Phys. Mech. Astron.* **65**, 278211 (2022).
- [51] H. Wu, Y. Wang, Y. Xu, P. K. Sivakumar, C. Pasco, U. Filippozzi, S. S. P. Parkin, Y.-J. Zeng, T. McQueen, and M. N. Ali, *The field-free Josephson diode in a van der Waals heterostructure*, *Nature (London)* **604**, 653 (2022).
- [52] Y. Zhang, Y. Gu, P. Li, J. Hu, and K. Jiang, *General theory of Josephson diodes*, *Phys. Rev. X* **12**, 041013 (2022).
- [53] N. Regnault *et al.*, *Catalog of flat-band stoichiometric materials*, *Nature (London)* **603**, 824 (2022).
- [54] D. Călugăru, A. Chew, L. Elcoro, Y. Xu, N. Regnault, Z.-D. Song, and B. A. Bernevig, *General construction and topological classification of crystalline flat bands*, *Nat. Phys.* **18**, 185 (2022).
- [55] J. Duan *et al.*, *Inventory of high-quality flat-band van der Waals materials*, *arXiv:2204.00810*.